JCBI
Journal of Computing & Biomedical Informatics
ISSN: 2710 - 1606
Volume 06 Issue 02
2024

Research Article
https://doi.org/10.56979/602/2024

A Multiclassification Framework for Skin Cancer detection by the concatenation of Xception and ResNet101

Ahmad Naeem[1*], and Tayyaba Anees[2]

[1]Department of Computer Science, School of Systems and Technology, University of Management and Technology Lahore, 54000, Pakistan.
[2]Department of Software Engineering, School of Systems and Technology, University of Management and Technology Lahore, 54000, Pakistan
Corresponding Author: Ahmad Naeem. Email: f2019288007@umt.edu.pk

Received: January 21, 2024 **Accepted:** February 27, 2024 **Published:** March 01, 2024

Abstract: Skin cancer is a deadly type of cancer that is responsible for millions of fatalities annually across the globe. This malignant cancer occurred due to the proliferation of abnormal epidermal cells, which subsequently spread to adjacent tissues and spread to other organs and tissues through the lymph nodes. Changes in lifestyle and sun-seeking behaviors have contributed to the increase in the incidence of skin cancer. It is critical to accurately identify and classify skin cancer to prevent the serious effects that result from delaying detection and treatment. This research paper presents a newly developed deep learning model that makes use of two advanced artificial intelligence techniques, Xception and ResNet101. This method attains an extraordinarily high degree of accuracy by using the special advantages of two strong networks. The Xception-ResNet101 (X_R101) model is capable of differentiating specific categories of skin cancers, such as melanoma (Mel), melanocytic nevus (Mn), basal cell carcinoma (bcc), squamous cell carcinoma (Scc), benign keratosis (Bk), Actinic keratosis (Ak), Dermatofibroma (Df) and Vascular lesion (Vl). The implementation of borderline SMOTE improves performance substantially. A comparison is performed between the proposed methodology and four benchmark classifiers: MobileNetV2 (BM3), DenseNet201 (BM4), InceptionV3 (BM1), and ResNet50 (BM2) and state-of-the-art classifiers. To evaluate performance of the proposed methodology, three publicly available datasets (PH2, DermPK and HAM10000) are utilized. The X_R101 model attains a prediction accuracy of 98.21%. The method's accuracy and effectiveness provide benefits to dermatologists and other healthcare practitioners in terms of timely identification of skin cancer.

Keywords: Skin cancer; Deep Learning; Melanoma; Medical imaging.

1. Introduction

Skin cancer is one of the deadliest types of cancer due to its high mortality rate. When the skin is exposed to a significant amount of ultraviolet (UV) radiation, the melanocyte cells present inside the skin undergo uncontrolled proliferation and this uncontrolled dispersion damages the healthy tissues [1]. The anomalous cells propagate throughout the lymph nodes, leading to the deterioration of neighboring tissues and the emergence of skin cancer [2]. A large number of the American population is suffering from this ailment which makes it a prominent public health issue. On an average about five million cases of skin cancer are diagnosed every year in the United States. [3]. The WHO reports that about 33% of all the deaths due to cancer are occurred by the skin cancer. Furthermore, there is a sharp rise in the number of skin cancer cases in the recent years [4]. A huge increase in the cases of skin cancer occur and the yearly mortality rate from skin cancer almost doubled since the 1990s [5]. Melanoma, a type of a skin cancer is the most dangerous for the human beings. Melanoma, considered as the highly malignant form of skin cancer, due to its high mortality. Annually, a very significant mortality rate from skin cancer has been linked with this particular type of melanoma occurring on the skin [6]. Skin melanoma comprises both benign and also

malignant skin cancers [7]. Melanoma (Mel), melanocytic nevus (Mn), basal cell carcinoma (bcc), squamous cell carcinoma (Scc), benign keratosis (Bk), Actinic keratosis (Ak), Vascular lesion (Vl) and Dermatofibroma (Df) are classified as non-melanoma skin malignancies [8]. In the USA, the second most commonly diagnosed kind of skin cancer is the basal cell carcinoma – 2.3 million of new cases of this type of cancer are reported annually. In most cases, they appear after melanoma and basal cell carcinoma have already appeared [8-9]. One of the leading causes of death in this type of skin cancer is its unusual detectability, mainly in cases of melanoma, a type of skin cancer which is curable only in the first stage [9]. The new cases of skin cancer and considering the fact that this problem is increasingly frequent, there is the need of more and more trained specialists in the diagnosis of this disease [10]. On the other hand, the present supply of such professionals seems to be embarrassingly inadequate [7]. Practically, there were 9,600 dermatologists who serviced the yearly number of 323 million people in the United States in 2018 [6]. Considering the scarcity of specialists responsible for providing accurate and timely diagnosis in the immediate term, innovative methodologies must be adopted [11].

Medical imaging is in the field for quite some time now and is proving beneficial to the experts. Medical imaging specialists have developed computer-aided detection (CAD) methodologies for a diverse range of medical conditions, encompassing skin cancer, foot ulcers, brain tumors, COVID-19 and several other ailments [12-15]. The essential CAD approach consists of four key components: input photo preprocessing, detection of infected area, feature extraction, and classification [16]. In the case of skin cancer, the validation of a dermatologist's manual diagnosis can be achieved by employing computer approaches to gain an additional assessment [17]. Numerous diagnostic approaches employ the ABCD rule, a framework that takes into account the attributes of symmetry, border irregularity, color variation, and dermatoscopic characteristics [18]. Skin cancer is frequently diagnosed by dermatologists utilizing these specific criteria. The presence of noise, low contrast, and irregular borders pose challenges in the recognition of melanoma photos [19]. According to the Melanoma Research Foundation, the reliability of the ABCD criteria for photograph-based melanoma diagnosis is questionable. Furthermore, an expert dermatologist is needed to perform these procedures otherwise an excessive number of false positive and false negative findings occur [20]. The aforementioned constraints highlight the necessity of exploring and advancing efficient automated skin cancer detection techniques for both inexperienced and experienced physicians. As a result, there has been an evolution of automatic approaches for detecting melanomas [21]. Computerized screening methods that utilize data extraction from dermoscopy images have proven to be beneficial in enhancing physicians' diagnostic capabilities [22]. There is an increasing trend in the utilization of various deep learning techniques such as CNN (convolutional neural network) by automated systems to independently extract data from input images [23]. Deep learning techniques are proving very effective in identifying diseases and categorizing images. Due to this the utilization of artificial intelligence (AI) models with enhanced diagnostic capabilities is being implemented in the domain of medical imaging [24].

In Section 2, an extensive examination is conducted on various deep learning and machine learning models that have been specifically designed for the accurate diagnosis of skin cancer and the identification of its subtypes. This research presents a unique deep-learning model named X_R101 that concatenates Xception and ResNet101 for feature extraction and multiclassification of skin cancer through the utilization of dermoscopy images. Furthermore, the utilization of the Borderline SMOTE technique effectively tackles the issue of class imbalance encountered in multiclassification tasks. The suggested model demonstrates a high level of efficacy in accurately classifying different forms of skin cancer in the early stages of the illness. This ultimately makes the lives of the healthcare professionals way easier since they can immediately respond by applying the necessary treatment procedures. The methodology applied in this research is centered on the application of the three open source PH2 [25], DermPK [26] and HAM10000 [27] datasets are combine together for the training and testing. The results demonstrated the supremacy of the proposed method above the available in marketplace approach in term of its detection accuracy, were obtained.

The following are the primary contributions of the study.

- An innovative and highly effective deep learning architecture called X_R101 is developed by fusing the Xception and ResNet101 networks.
- The proposed network classifies the dermoscopy images into eight distinct classes: Mel, Mn, Bcc, Scc, Vl, Ak, Df and Bk.

- The proposed X_101 model has the ability to efficiently detect skin cancer by employing dermoscopy images. This model exhibits exceptional effectiveness in real-life situations. Its efficacy has been assessed utilizing combined data consist of PH2, DermPk and HAM10000 datasets, which are available to the public.
  Furthermore, the novel X-R101 model integrates an efficient computational framework, in addition to gathering features from two renowned networks, Xception and ResNet101. The network undergoing assessment demonstrates exceptional performance on a dataset, achieving a maximal accuracy rate of 98.21%.
- After performing an McNemar statistical test, it is apparent that the X_R101 model exhibits a higher level of performance in comparison to the remaining models.

The main points of the article are briefly summarized as follows. In the following section 2, a literature review is discussed on the ML/DL algorithms for skin cancer detection. The current methodology utilized a combined dataset consist of PH2, DermPk & HAM10000 dataset that is described in greater detail in Section 3. In Section 4, the experimental configuration and results are described in detail. The discussions are provided in Section 5. In Section 6, the conclusion and potential limitations are discussed.

2. Literature Review

Depletion of the ozone layer over time has been recognized as a factor in the increase in the incidence of skin cancer. As a result, researchers have been actively developing automated systems to examine dermoscopic images with the aim of identifying indicators of skin cancer. The methods utilized are ML, DL and computer vision-derived. In the section that follows, the methodologies proposed in the relevant research are discussed as shown in Table 1.

Kaseem et al [28]. proposes a method for properly categorizing skin lesions. Using transfer learning and a pre-trained GoogleNet model, the proposed model was constructed. The model's starting parameters will likely shift as a result of the training process. The widely known public challenge dataset, ISIC 2019, is used to test the suggested approach. Accurate diagnosis of 8 different classes of skin cancers including melanomas, melanocytic nevi, basal cell carcinomas, actinic keratoses, benign keratoses, dermatofibromas, vascular lesions, and squamous cell carcinomas was made possible by the proposed model. Precision was 80%, sensitivity was 79.82%, specificity was 97%, and accuracy in classifying was 94.92%. The model can identify photographs that do not fall inside any of the predefined eight classifications. In such cases, these images are categorized as unknown images.

Abbas et al. [29] conducted a study in which they compared dermoscopy and deep learning for melanoma classification. This paper introduces a deep-learning skin cancer categorization model. Yonsei University Health System's dermoscopy images database was used in their investigation. Image processing and data augmentation have created a reliable automated AM detection system. This study uses a seven-layer deep convolutional network. The class started without weights or settings. Their model was evaluated using transfer learning in this study. After changes, AlexNet and ResNet-18 were fine-tuned and trained on the same dataset. The proposed technique improved benign nevi and AM accuracy by 90%. They achieved over 97% accuracy using transfer learning, which is equivalent to cutting-edge approaches. Their algorithm correctly recognized skin cancer instances after a comprehensive investigation. Dermatologists may apply the suggested technique to make data-supported clinical choices on early A.M. detection, according to our research.

Reis et al. [30] introduced InSiNet, a CNN that uses deep learning to distinguish benign as well as malignant tumors. The technique's efficacy is tested in a controlled environment utilizing images from the International Skin Imaging Collaboration's 2018–2020 investigations. The suggested technique was compared to GoogleNet, DenseNet-201, ResNet152V2, EfficientNetB0, RBF-support vector machine, logistic regression, and random forest for computational speed and accuracy. The InSiNet architecture outperformed other architectures on the 2018–2020 ISIC datasets. InSiNet achieved 94.59%, 91.89%, and 90.54% accuracy for ISIC 2018, 2019, and 2020 datasets, respectively.

Monika et al [31] in their research aim to identify and classify skin cancer using machine learning and image processing. Pre-processing includes dermoscopy images. After removing unwanted hair on the skin lesion with a dull razor, a Gaussian filter smooths the image. Lesion boundaries are kept, and median filters remove noise. Because color contributes to cancer examination, the classification approach uses

color-based k-means clustering. GLCM and ABCD are used to derive texture traits. The clinical study uses ISIC 2019 Challenge dataset comprising eight dermoscopic image types. The Multi-class Support Vector Machine (MSVM) was categorized with 96.25 percent accuracy.

Ibraheem et al [32]. enhanced the lesion images by employing the contrast-limited adaptive histogram equalization (CLAHE) method. In this, threshold equalization and bilinear interpolation were the two crucial elements. On top of that, a process based on pixels was employed to divide the skin lesions and reclaim their inherent characteristics. The categorizations ranged from 0 (which designated a background item) to 2 (which denoted melanoma), with 1 (which denoted a benign tumor) as the lowest classification. Gradient Boosted Tree (GBT) attained 97.5 percent accuracy.

From visual features, Rehman et al. [33] used convolutional neural networks (CNN) to detect malignancy. The dataset utilized in the International Skin Collaboration (ISIC) 2016 study consisted of instructional photographs possessing a size of 1024 by 767 pixels These photos came in three different varieties; melanoma was labeled as malignant, nevus and seborrhea keratosis as benign. This study employed a convolutional neural network (CNN) to be represented by Rectified Linear Units (ReLU) for image categorization. In addition, the extended Gaussian distribution is also used in the context of image segmentation. Accuracy, specificity, and sensitivity were metrics that showed the effectiveness of the model. The approach suggested has a 98.32% chance of success, which does not have any independently verified data yet. Data augmentation technique was used in the article by Shetty et al [34]. The adopted approach of the k-fold cross-validation tested model makes a better model more robust. Convolutional Neural Network (CNN) showed higher accuracy in the study results than other machine learning algorithms. When we employed CNN model, the proposed proposal gave the highest accuracy score (95.18%).

Agbenieme et al. [35] used Convolutional Neural Networks (CNNs) to classify seven types of cutaneous carcinoma into DenseNet201. Several pre-processing and analysis steps were done before categorizing the given image samples of skin lesions. We implemented tests of both the ISIC 2017 and HAM10000 datasets to estimate the accuracy of the adopted classification system. The proposed method accuracy of the test is 86.1% and the training accuracy is 99.12%. Naeem et al [36] developed an extraordinary model called SCDNet used to distinguish among the different categories of skin cancer whereby a combination of Vgg16 and CNN is applied. When considering the task of classifying skin cancer, the SCDNet showed a classification precision of 96.91%.

Based on a study that was run which looked at four different deep learning techniques of Xception, ResNet50, CNN and RNN by Singh et al.[37], it is necessary to discover the best trusted method for sickness predictions. This study was performed on dataset HAM10000. As the research shows, the CNN, RNN, ResNet50, and Xception methods are more efficient than the traditional methods with accuracy rates of 72%, 69%, 73%, and 93% well.

Table 1. Literature Review

Method	Dataset	Accuracy	Year	Ref
Transfer Learning + Google net	ISIC 2019	94.92%	2020	[28]
AlexNet + ResNet-18	Yonsei University Health System's dermoscopy images database	97.00	2021	[29]
InSiNe	ISIC 2018 ISIC 2019 ISIC 2020	94.90 91.89 90.54	2022	[30]
MSVM	ISIC2019	96.25	2020	[31]
GBT	ISIC2019	97.50	2020	[32]
CNN based model	ISIC 2016	98.32	2018	[33]

CNN	HAM10000	95.18	2022	[34]
DenseNet201	ISIC 2017 + HAM10000	86.10	2022	[35]
SCDNet	ISIC 2019	96.91	2022	[36]
CNN	HAM10000	72.00	2022	[37]
RNN		69.00		
ResNet50		73.00		
Xception		93.00		

3. Proposed Methodology

This section explores the extensive workflow of the system under consideration. The Figure 1 illustrates the proposed model and provides a comprehensive sequence from dataset collection to experimental results.

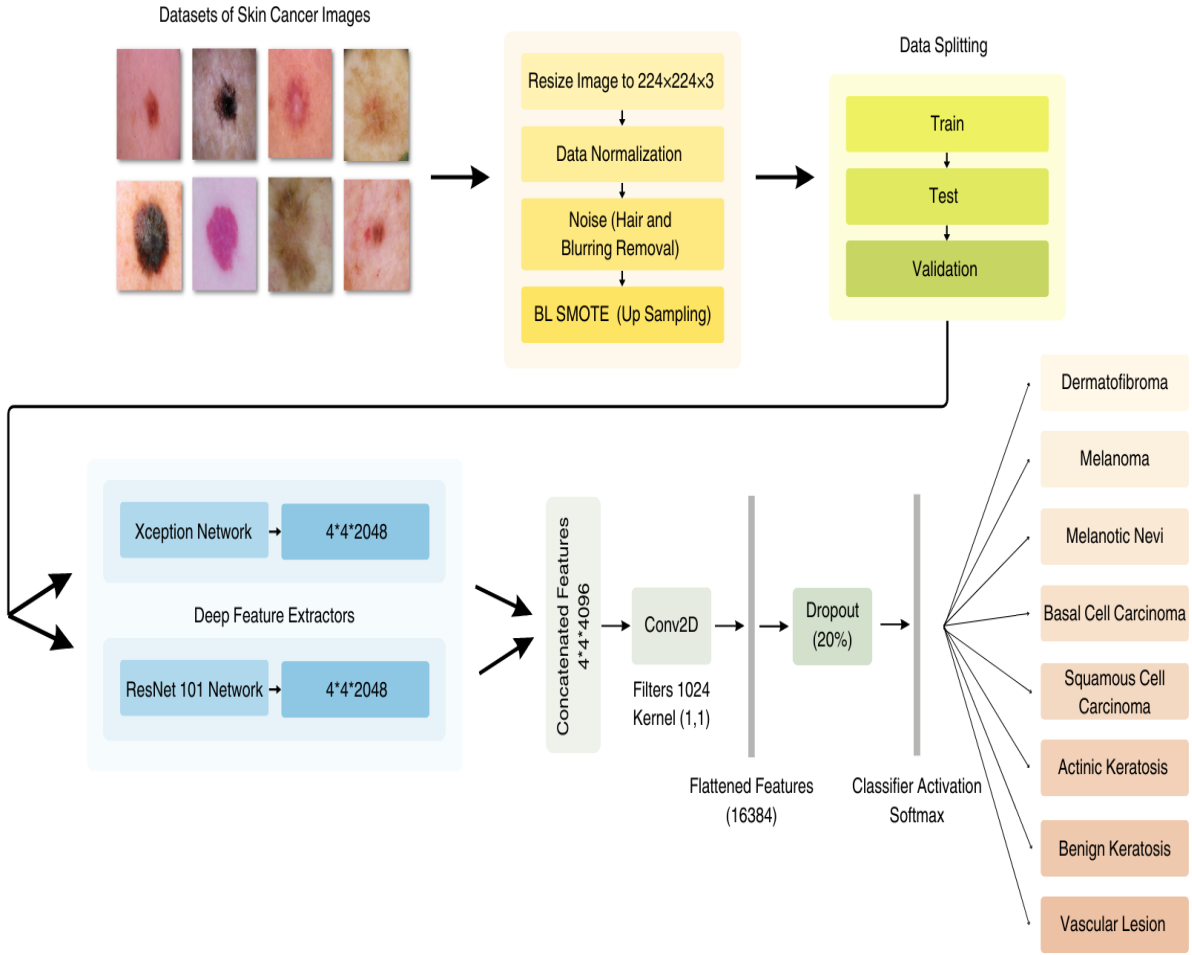

Figure 1. Proposed Methodology

3.1 DataSet

3.1.1. Dataset Description

The model is trained by utilizing publicly available PH2[25], DermPk[26] and HAM10000 [27] datasets. These datasets comprise of diverse and accurately curated collection of high-quality skin lesion images, replete with rich metadata, which helps in skin cancer classification and clinical decision support. The combined dataset encompasses major classes including melanoma, melanocytic nevi, basal cell carcinoma, actinic keratosis, squamous cell carcinoma, dermatofibroma, vascular lesion, and seborrheic keratosis as describe in table 2. These images, empower researchers to explore the intricacies of dermatological conditions as shown in Figure 2.

This paper uses these datasets in advancing dermatological research and machine learning model creation. The images included in this dataset proved to be very valuable in training and validating the proposed model.

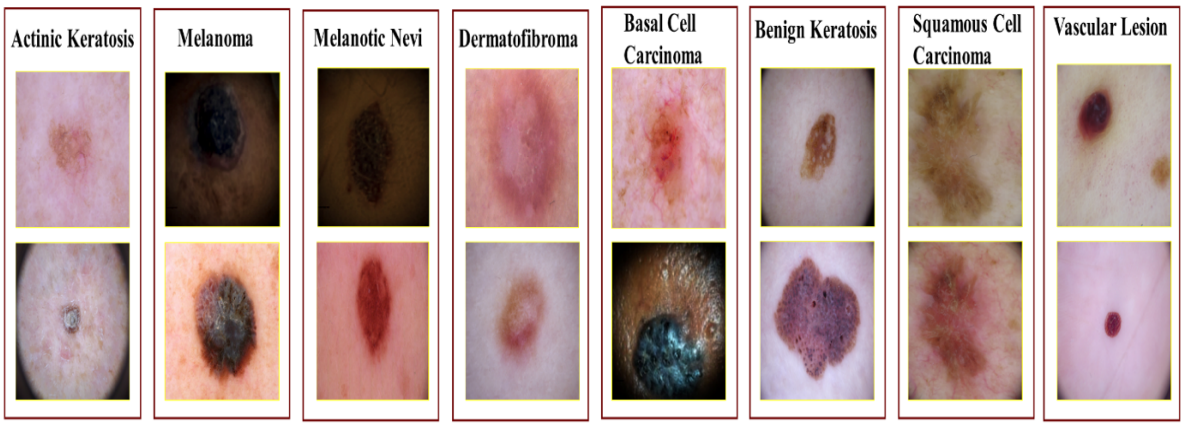

.

Figure 2. Sample Images from Dataset

Table 2. Image Distribution of Datasets

Class	PH2	DermPK	HAM10000	Total Number of Images
Melanoma	40	30	1113	1183
Melanocytic nevus	-	35	6705	6740
Basal cell carcinoma	-	40	514	554
Squamous cell carcinoma	-	29	-	29
Benign keratosis	80	15	1099	1194
Actinic keratosis	-	-	327	327
Dermatofibroma	-	-	115	115
Vascular lesion	-	-	142	142

3.1.2. Balancing the dataset

The BODERLINE-SMOTE methodology is a variant of the SMOTE method proposed by Han et al. [38] The method initiates by categorizing the observations that pertain to the minority class. Given the premise that the dominant class encompasses the entirety of the environment. In instances of this nature, any observation that arises from the minority class will be categorized as noise and will not be utilized for the purpose of generating synthetic data, since it will be considered inconsequential. Furthermore, the process involves the discernment of a limited set of particular regions referred to as "border spots," which are characterized by their positioning amidst the dominant and marginalized communities. The sample technique subsequently concentrates exclusively on the aforementioned chosen sites. Consequently, the Borderline-SMOTE technique is employed to augment the quantity of occurrences in the dataset photographs. The present study utilizes the seven-category classification system of the HAM10000, three categories of Ph2 and Six categories of DermPK. The aforementioned classifications include melanoma, melanocytic nevus, basal cell carcinoma, actinic keratosis, squamous cell carcinoma, dermo fibroma, vascular lesion, and seborrheic keratosis. Following a subsequent step known as up-sampling, a dataset is augmented by the addition of a total of (no. of images before applying smote) samples. Upon the successful implementation of the Borderline-SMOTE technique, the quantity of photographs within each class experienced a notable increase, resulting in a total count of (no. of images after applying smote) images as shown in table 3.

Table 3. Image Distribution after Bl-SMOTE

Class	Selected Images	Images after Bl-SMOTE
Melanoma	460	1200
Melanocytic nevus	500	1200
Basal cell carcinoma	400	1200
Squamous cell carcinoma	29	1200
Benign keratosis	400	1200
Actinic keratosis	327	1200
Dermatofibroma	115	1200
Vascular lesion	142	1200

3.1.3. Data Preprocessing (Gaussian filtering)

To enhance image quality and reduce noise as shown in figure 3, we harnessed the power of 2D Gaussian filters. While these filters imposed considerable computational demands, they also ushered in a novel realm for research exploration. In this sub-stage, Gaussian operators took on the role of convolutional operators, advocating the adoption of convolution for efficient smoothing [39].

$$Gus_{1c^{(i)}} = \frac{1}{\sqrt{2\pi\sigma}} e^{-\left(\frac{i^2}{2\sigma^2}\right)} \quad (1)$$

To accomplish localization, the smoothing procedure employs a substantial filter that operates in both the frequency and spatial domains. The aforementioned depiction is also employed to operationalize the concept of uncertainty.

$$\Delta i \Delta \mu \geq \frac{1}{2}, \quad (2)$$

The mathematical representation of the two-dimensional operator for a Gaussian filter is provided below.

$$Gus_{2c^{(i,\ j)}} = \frac{1}{2\pi\sigma^2} e^{-\left(\frac{i^2+j^2}{2\sigma^2}\right)} \quad (3)$$

Within the given context, the standard deviation of a Gaussian function is denoted by the symbol sigma (σ). The highest point of the value corresponds to the point at which the smoothing effect is most pronounced. The positional information of the image, denoted by the Cartesian coordinates i and j, can be utilized for the purpose of determining the dimensions of the window. Moreover, are also resized and normalized to achieve better classification results.

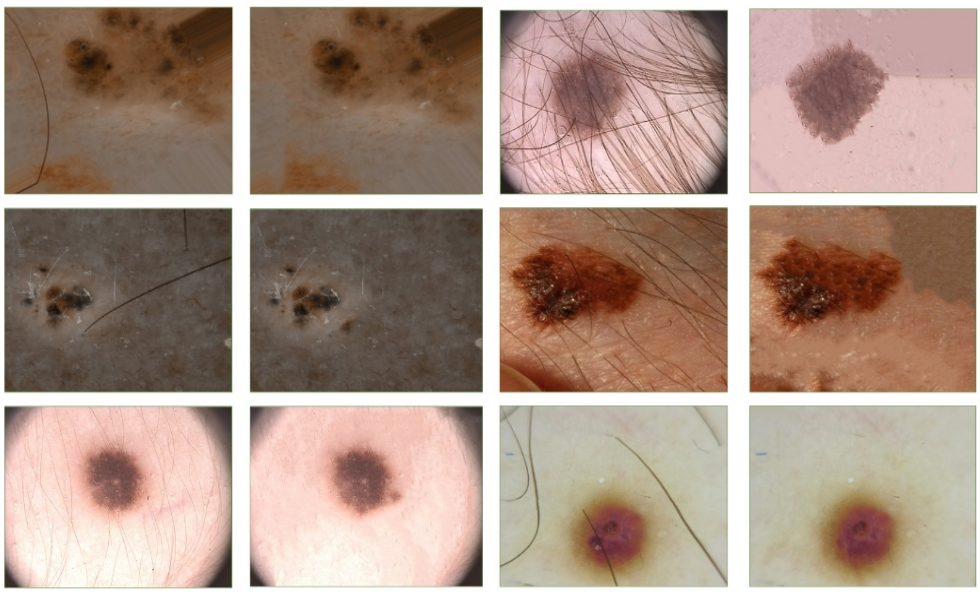

Figure 3. Images after Preprocessing

3.1.4. Xception Net

In the deep Xception Network model, pointwise convolutional layers are utilized to generate additional inception layers followed by the convolutional layers. When the Xception framework is implemented, the depthwise separable convolutions of InceptionV3 are modified. Spatial convolution is accomplished through the utilization of depthwise convolution channels that possess the dimensions $a \times a$. In order to perform pointwise convolution, each dimension must be transformed individually. A convolutional operation is implemented by Xception to merge features in both the depthwise and pointwise directions. In contrast to Xception, Inception applies non-linear activation after convolution [40].. Xception as a whole utilizes a cumulative total of 23 million parameters distributed throughout in its 71 layers.

3.1.5. Resnet101

A wide range of research results has been compiled relating the versatility of Residual Networks (ResNet) in the domain of computer vision [41, 42]. It has been established that this network is capable of training with a maximum depth of one thousand layers [43]. The ResNet 101 architecture enables uninterrupted information transmission between layers by employing the correlation principle among identical connections [44]. The CNN model operates at a relatively swift rate and utilizes a reduced number of parameters. By effectively addressing vanishing gradients, this convolutional neural network (CNN) structure attains enhanced accuracy and quicker convergence. For the purpose of streamlining this network model, shortcut connections are employed instead of the convolutional layers block approach . When the input and output dimensions are identical, the shortcut connections method, which was recently introduced, is utilized. When confronted with situations that involve multiple dimensions, there are two viable methodologies to choose from. In order to enable shortcut mappings, identity mapping first adds zeros to the dimensional increment; as a result, there will be no parameter increase. The second methodology achieves input and output dimension alignment through the utilization of a projection shortcut in conjunction with 1.0 convolutional filters. The proposed architecture's increased complexity and ResNet-101's dependence on Batch Normalization layer execution are the two most frequent implementation-related issues. The following equation serves as a fundamental component in this model*:*

$$K = F(J, \{M_n\}) + J \tag{4}$$

J and *K* are the input and output vectors where $F(J, \{M_n\})$ is the mapping function to be learned whereas *J* + *K* are performed by the shortcut connections.

The pre-trained model was utilized to perform image identification. This model incorporates 104 batch normalization layers, 100 ReLU layers, 104 convolutional layers, SoftMax, entirely connected, average pooling, and max polling, in addition to the 33 additional layers specified below. The model was provided with an image that had the subsequent dimensions: 224 x 224 x 3. The parameters utilized by the max-polling operation of this model are padding (0,1,0, and 1), pool size (3,3) and stride (2,2). Without padding, the standard pooling operation utilizes a (7,7) pool and stride size. After the network training procedure is complete, the acquired features are obtained through the utilization of the PH2 and DermPK datasets. A grand total of one thousand features were chosen from the 'fclayer' layer, whereas 2048 features were obtained from the 'pool5' layer.

3.2 Proposed method: Concatenated X_R101

The research paper presents the concatenated X_R101 model, which demonstrates efficacy and accuracy in the classification of a wide variety of skin lesions named basal cell carcinomas, vascular lesions, melanomas, melanocytic nevi, dermatofibromas, actinic keratoses, and intraepithelial carcinomas. The graphical structure of the concatenated network is depicted in Figure 8. A noticeable improvement in the precision of predictions generated by the model is observed. The unified X_R101 achieves classification and standard feature extraction within a single frame by manipulating the quantity of concealed layers. The pre-processed skin photos from the datasets are resized to the resolution of 224 by 224 pixels. In the final phase of feature extraction, feature maps with the 4 × 4 × 2048 dimensions are produced by Xception and ResNet101. The feature maps under consideration are derived from the input image. Based on the similarity observed in the feature maps generated by both models, it is viable to merge them in a way that

optimizes the utilization of the inception and residual layers, resulting in semantic features of higher quality. In order to construct a concatenated deep network, the classifier is utilized in conjunction with the features extracted from Xception and ResNet101 via the convolutional layer. In addition to the convolutional layer with 1024 filters, a 1 x 1 kernel is also incorporated. The function for activation does not exist. By utilizing the convolutional layer, the network is capable of efficiently extracting significant semantic features from the aggregated data across all channels. The core element of the proposed framework comprises an improved system for predicting skin cancer that is characterized by its uncomplicated architecture. By concatenating the initial X_R101 layer, the dimensions of the input image are reduced to 128 by 128 pixels. Eight unique classification categories are generated as a result of the operation. The activation functions Softmax and ReLu were applied to the model's output in order to populate the hidden layer. During the entirety of the training process, a 20% withdrawal rate was mandatory to prevent the occurrence of overfitting.

3.3 Performance Metrics

This procedure of the model evaluation was based on several metrics, including F1-score, recall, accuracy, and precision. The success or failure were tested by using the true positives (TP), false positives (FP), true negatives (TN), and false negatives (FN). The quantities of photographs that were mistakenly identified as other malignant images (FP), FN which are normal images misclassified as some disease, and the TN which are correctly labelled as some disease due to normal images and images that are correctly identify is donated as (TP) . The precision is defined as the ratio of the correct instances to the total number of the set of images that are ranked. The mathematical forms of these measures are as follows:

$$\text{Accuracy} = \left(\frac{TP+TN}{TP+FN+FP+TP}\right) \quad (5)$$

$$\text{Precision} = \left(\frac{TP}{TP+FP}\right) \quad (6)$$

$$\text{Recall} = \left(\frac{TP}{TP+FN}\right) \quad (7)$$

$$\text{F1-Score} = 2 * \left(\frac{Precesion*Recall}{Precesion+Recall}\right) \quad (8)$$

4. Experimentation Results

In the section that follows, we assess X_R101 to the most recent CNN classifiers. This section discusses the distinctions among the suggested X_R101 and the four well-known CNN networks.

4.1. Experimental Setup and Hyper-Parameter's Fine Tuning

The development of the suggested model was performed utilizing version 2.12.0 of TensorFlow (TF). TF version 1.8 was employed for the construction of the four baseline CNN networks (BM1, BM2, BM3, BM4). Using Python 3.10.1, methods that are not limited to convolutional networks were developed. The study was performed on an individual computer operating on the Windows 10 operating system, featuring 32 GB of RAM and a 12 GB NVIDIA GPU. A comprehensive summary of the critical hyperparameters that regulate the functioning of the X_R101 architecture is provided in Table 4.

Table 4. List of the X_R101 Architecture's implemented hyper-parameters.

Parameter Name	Type
Learning Rate	0.001
Batch size	32
Call back	ReduceLROnPlateau
Epochs	30
Optimizer	RMSprop

Activation function (Hidden layer)	ReLU
Activation function (Output layer)	SoftMax

The X_R101 model exhibits the capability of differentiating among six distinct types of skin cancer by integrating dermoscopy images. In order to optimize the X_R101 model, adjustments were made to its hyper-parameters, namely the learning rate, epoch and batch size, through the implementation of grid search. To optimize the development process of the Proposed X_R101, a batch size of 32 and a maximum of 30 testing epochs were implemented. Utilizing the stochastic gradient descent (SGD) optimizer, the learning rates (LR) for the four CNN networks and the proposed X_R101 were initially set to 0.05. After twenty unsuccessful iterations of training, a reduction of 0.1 was made to the LR parameter. Given the potential for substantial consequences that could arise from overfitting the input data, this measure was taken to protect the X_R101 model and four CNN networks.

4.2. Accuracy of the Proposed X_R101 in Comparison to Other Classifiers

Our model's accuracy is assessed in terms of the proportion of correct predictions it produces. Upon applying the BL-SMOTE techniques to the dataset, X_R101 is contrasted with four additional widely recognized CNN networks. The results obtained by applying the BL SMOTE method to the proposed model were exceptional. The accuracies achieved for the X_R101 models, comprising four baseline models BM1, BM2, BM3 and BM4 are detailed in Table 5. The corresponding values were 92.14%, 93.95%, 95.48%, 96.67%, 92.98% and 98.21% for BM1, BM2, BM3, BM4, X_R101 and X_R101 With BL SMOTE. The primary differentiation of the proposed X_R101 is accomplished by employing the BL SMOTE, as illustrated in Figure 4.

Table 5. Evaluation of proposed X_R101 with four CNN networks.

Classifiers	Accuracy	Precision	Recall	F1-score	AUC
BM1	92.14%	92.26%	92.20%	92.23%	98.16%
BM3	93.95%	93.93%	93.89%	93.91%	98.29%
BM3	95.48%	95.60%	95.70%	95.65%	98.34%
BM4	96.67%	96.72%	96.79%	96.73%	98.40%
Proposed X_R101 (Without BL-SMOTE)	92.98%	93.10%	93.01%	93.05%	96.93%
Proposed X_R101 (With BL-SMOTE)	98.21%	98.41	98.33%	98.37%	99.29%

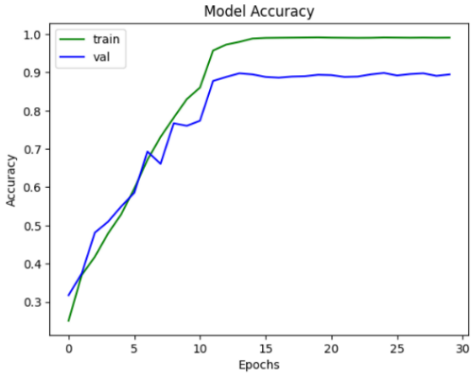

BM 1

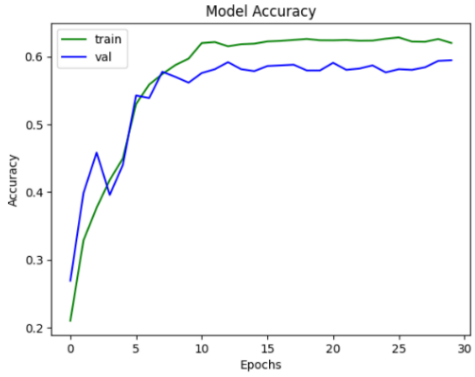

BM 2

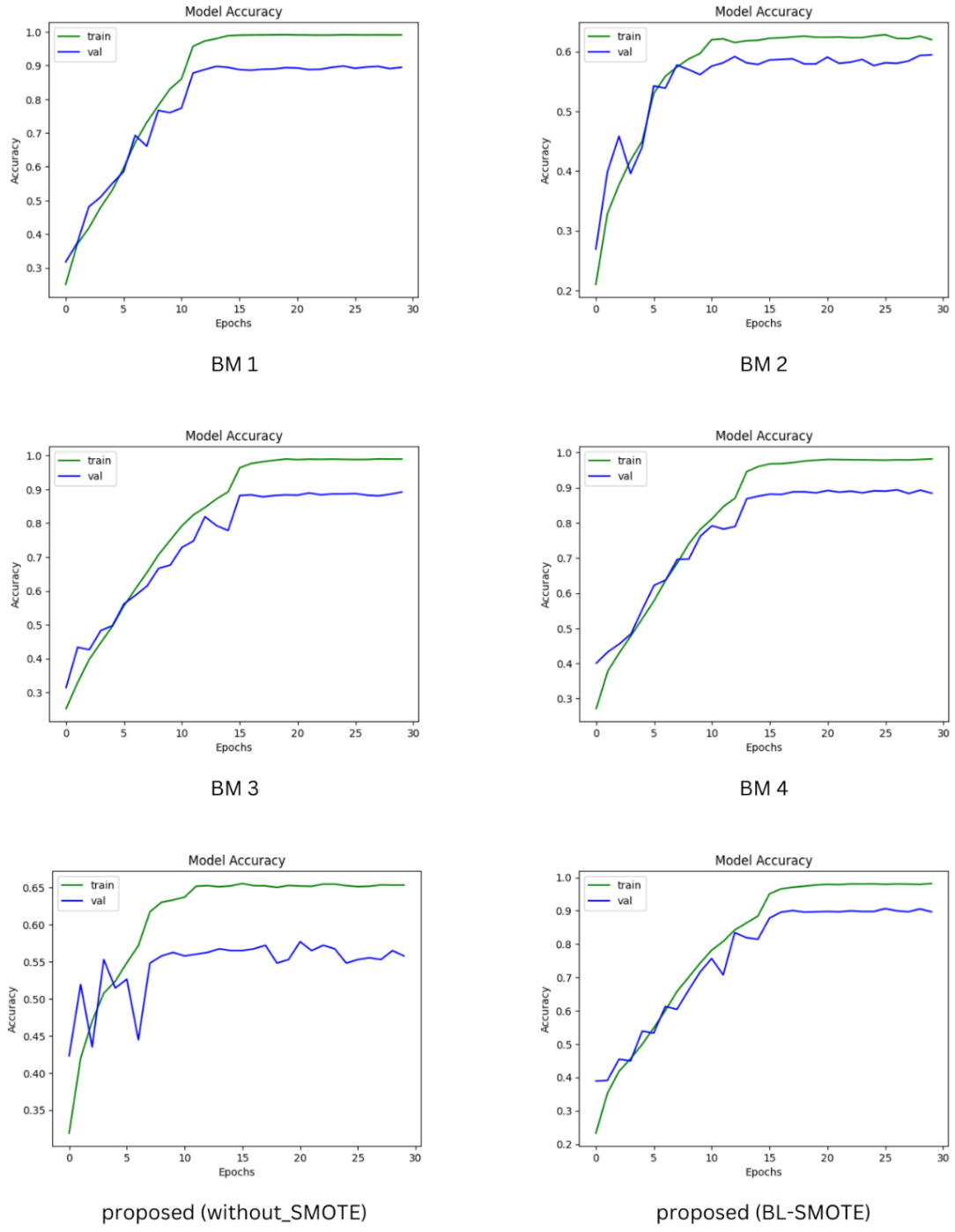

Figure 4. Comparison of Proposed X_R101 to baseline networks using accuracy (a) BM1 (b) BM2 (c) BM3 (d) BM4 (e) Proposed X_R101 before Borderline SMOTE, (f) Proposed X_R101 using Borderline SMOTE Tomek.

4.3. Loss of the Proposed X_R101 in Comparison to Other Classifiers

The loss function is utilized to calculate the amount of discrepancy that exists between the predicted and observed values. In this investigation, the magnitude of the loss was determined by employing a categorical cross-entropy methodology. The results became considerably more apparent subsequent to the construction of the X_R101 model utilizing upsampled images. The proposed X_R101 models produced loss values of 0.5101 and 0.8010 respectively, when assessed with and without BL SMOTE TOMEK. The loss values corresponding to BM1, BM2, BM3, and BM4 are as follows: 0.6819, 0.9829, 0.6534 and 0.6040

respectively. As shown in Figure 5, BL SMOTE has significantly reduced the loss value of the X_R101 system under consideration.

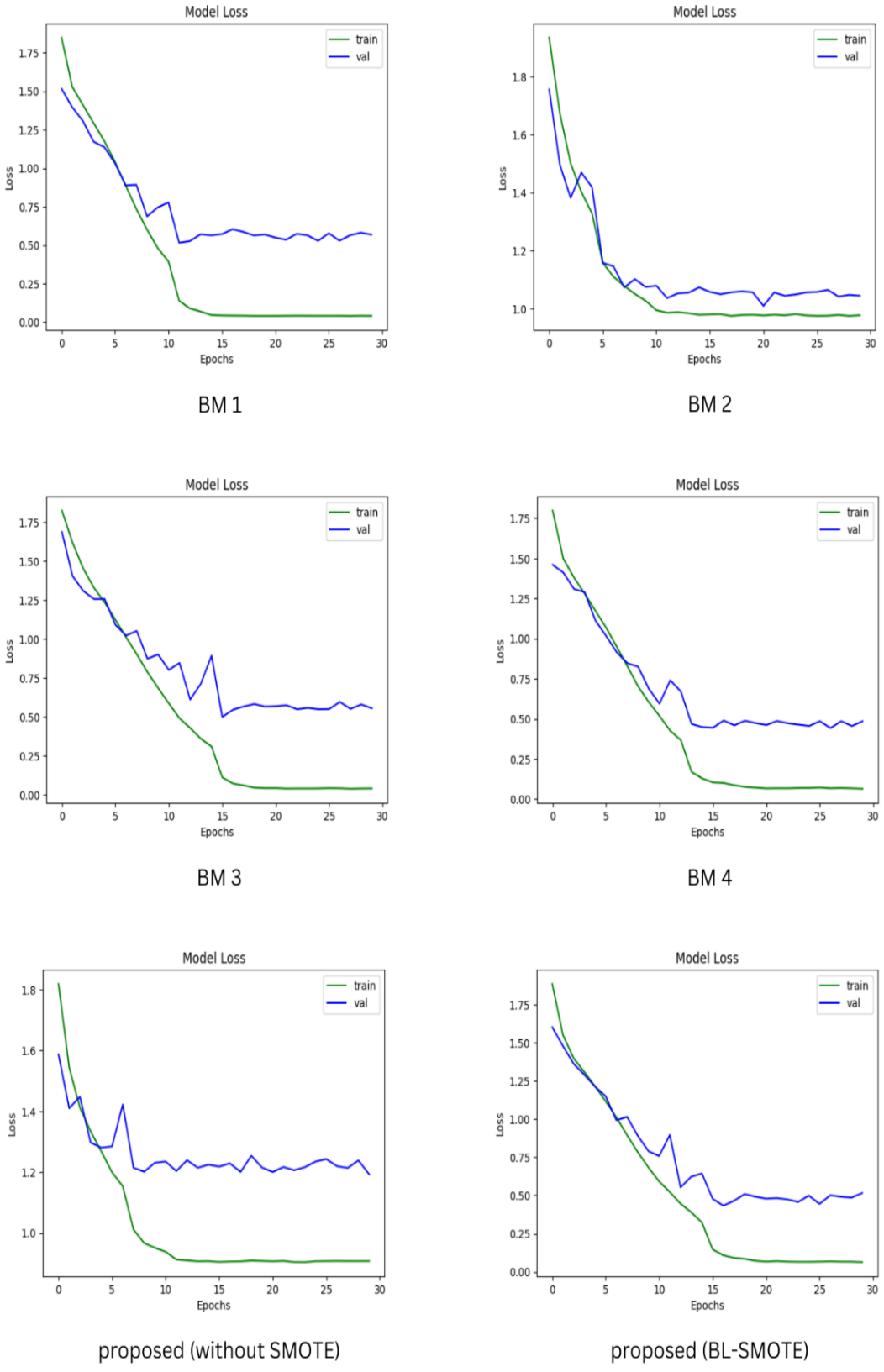

Figure 5. Contrasting of Proposed X_R101 to baseline networks using loss values (a) BM1 (b) BM2 (c) BM3 (d) BM4 (e) Proposed X_R101 before Borderline SMOTE, (f) Proposed X_R101 using Borderline SMOTE Tomek.

4.4. F1-score of the Proposed X_R101 in Contrast to Baseline Networks

The proposed X_R101 model standardizes the input samples by using the one-hot encoder is that integrates classified data into variables. In order to address the issue of an imbalanced dataset, the methods of oversampling, BL-SMOTE is utilized to bring the dataset into balance. The utilisation of BL SMOTE substantially enhances the F1-score of the proposed X_R101, as illustrated in Figure 6. In the presence and absence and BL-SMOTE, the F1 scores for the proposed X_R101 models were 98.37% and 93.05% respectively. Conversely, the F1-scores of BM1, BM2, BM3, and BM4 were as follows: 92.23%, 93.91%, 95.65% and 96.73% respectively. The principal differentiation introduced by the incorporation of BL SMOTE into the proposed X_R101 is illustrated in Figure 6.

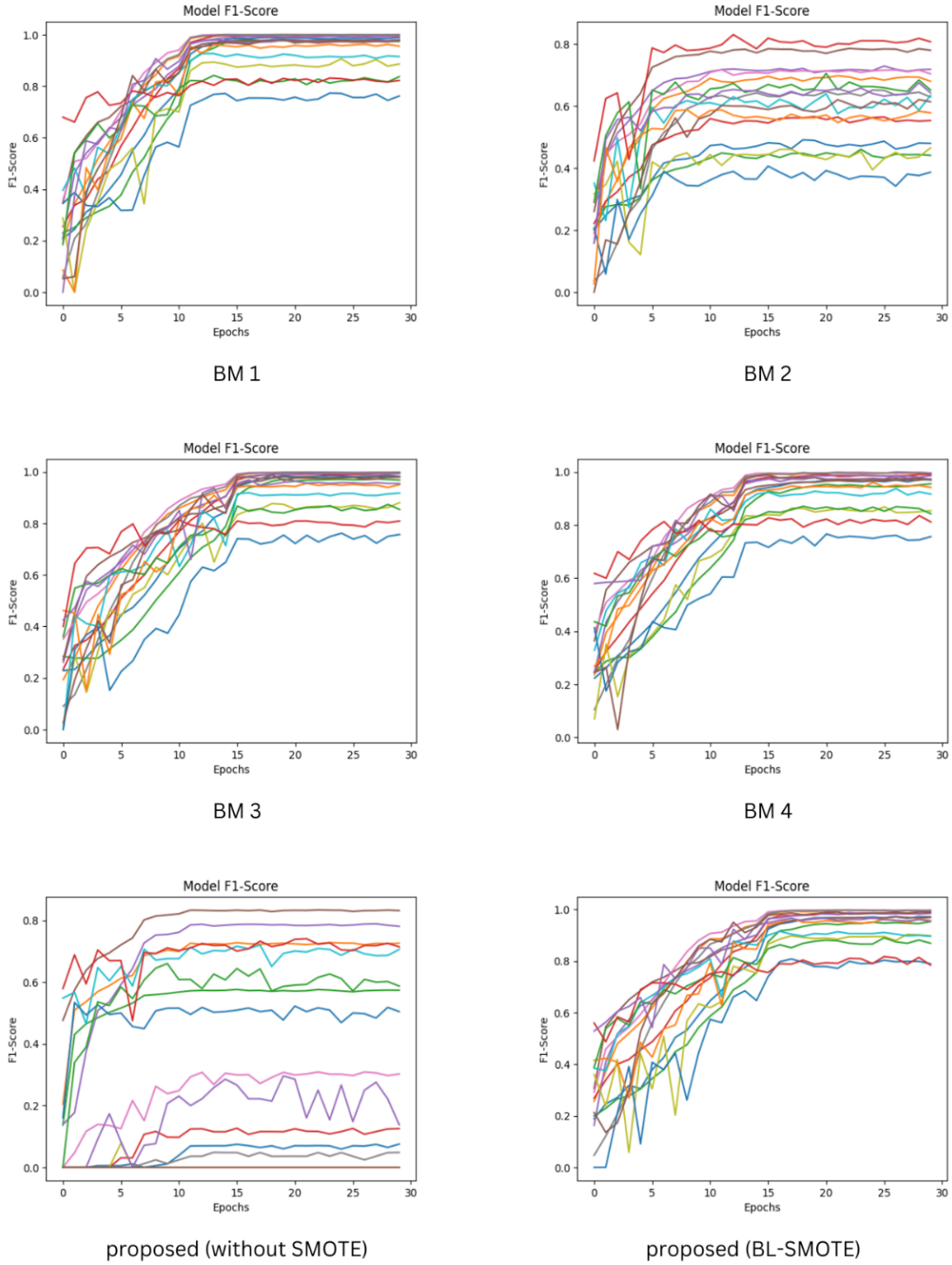

Figure 6. Evaluation of Proposed X_R101 to baseline networks using F1-score (a) BM1 (b) BM2 (c) BM3 (d) BM4 (e) Proposed X_R101 before Borderline SMOTE, (f) Proposed X_R101 using Borderline SMOTE Tomek.

4.5. Recall of the Proposed X_R101 in Comparison with Other Classifiers

The recall criterion was incorporated in order to assess the model's ability to accurately identify positive samples. Undoubtedly, the higher recall values resulted in the acquisition of a greater quantity of positive samples. The outcomes of a recall curve comparison between the proposed X_R101 and four baseline models are depicted in Figure 7. The recall values for the X_R101 model with and with BL Smote, BM1, BM2, BM3, and BM4 derived from the gathered data were as follows: 98.33%, 93.01%, 92.20%, 93.89%, 95.70% and 96.79%%. After this explanation, the proposed method promptly established its remarkable efficiency.

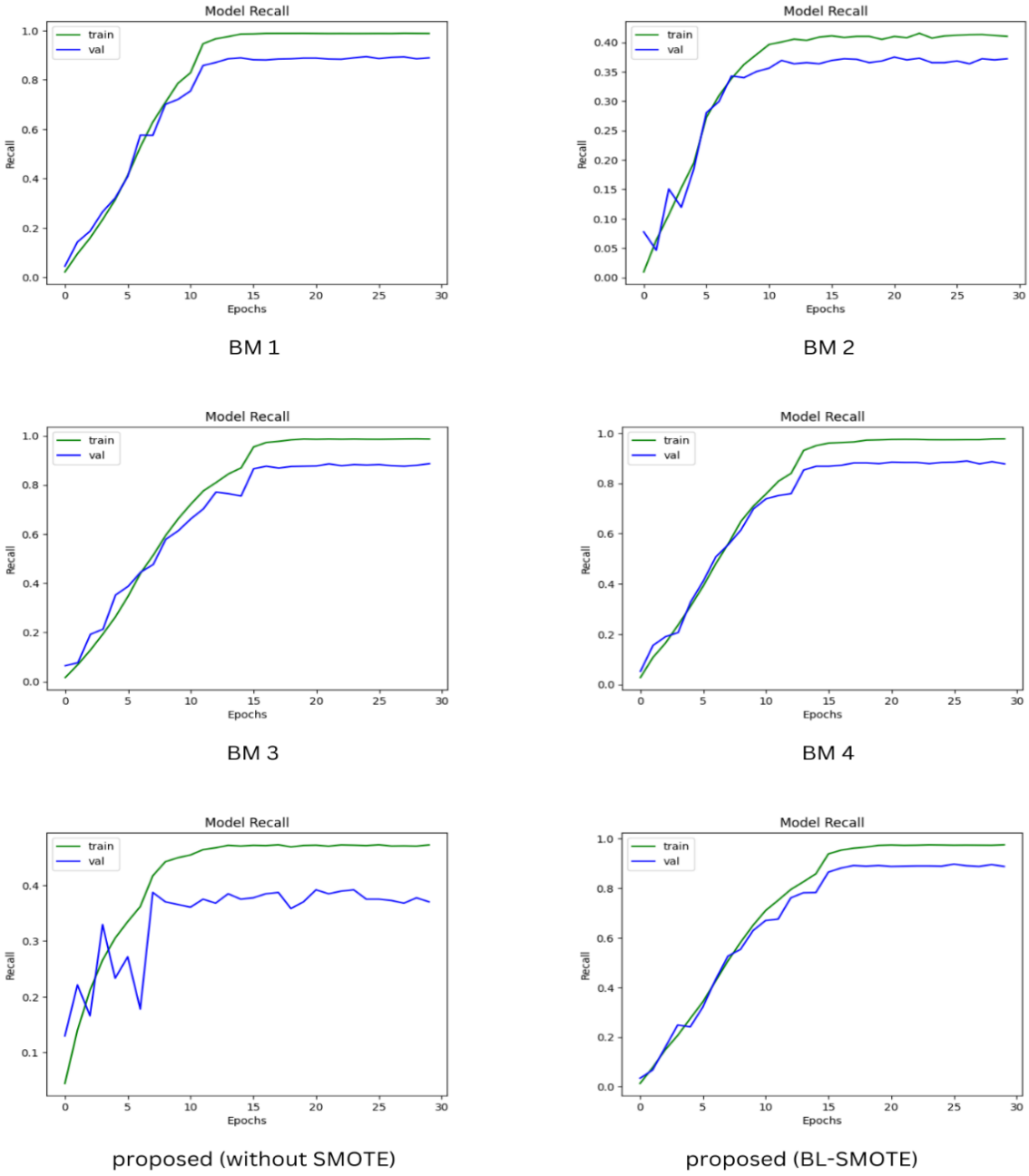

Figure 7. Comparison of Proposed X_R101 to baseline networks using recall value (a) BM1 (b) BM2 (c) BM3 (d) BM4 (e) Proposed X_R101 before Borderline SMOTE, (f) Proposed X_R101 using Borderline SMOTE Tomek.

4.6. AUC of the Proposed X_R101 in Contrast to Baseline Networks

We evaluate our proposed model against four other well-known CNN networks by analyzing the datasets before and after SMOTE TOMEK and BL-SMOTE integration. The utilization of BL SMOTE

significantly improves the area under the curve (AUC) of the proposed X_R101, as depicted in Figure 8. When assessed with and without BL-SMOTE, the AUC values for the proposed X_R101 models were as follows: 99.29%, 96.93% respectively. BM1, BM2, BM3, and BM4 had respective AUC values of 98.16%, 98.29%, 98.34%, and 98.40%.

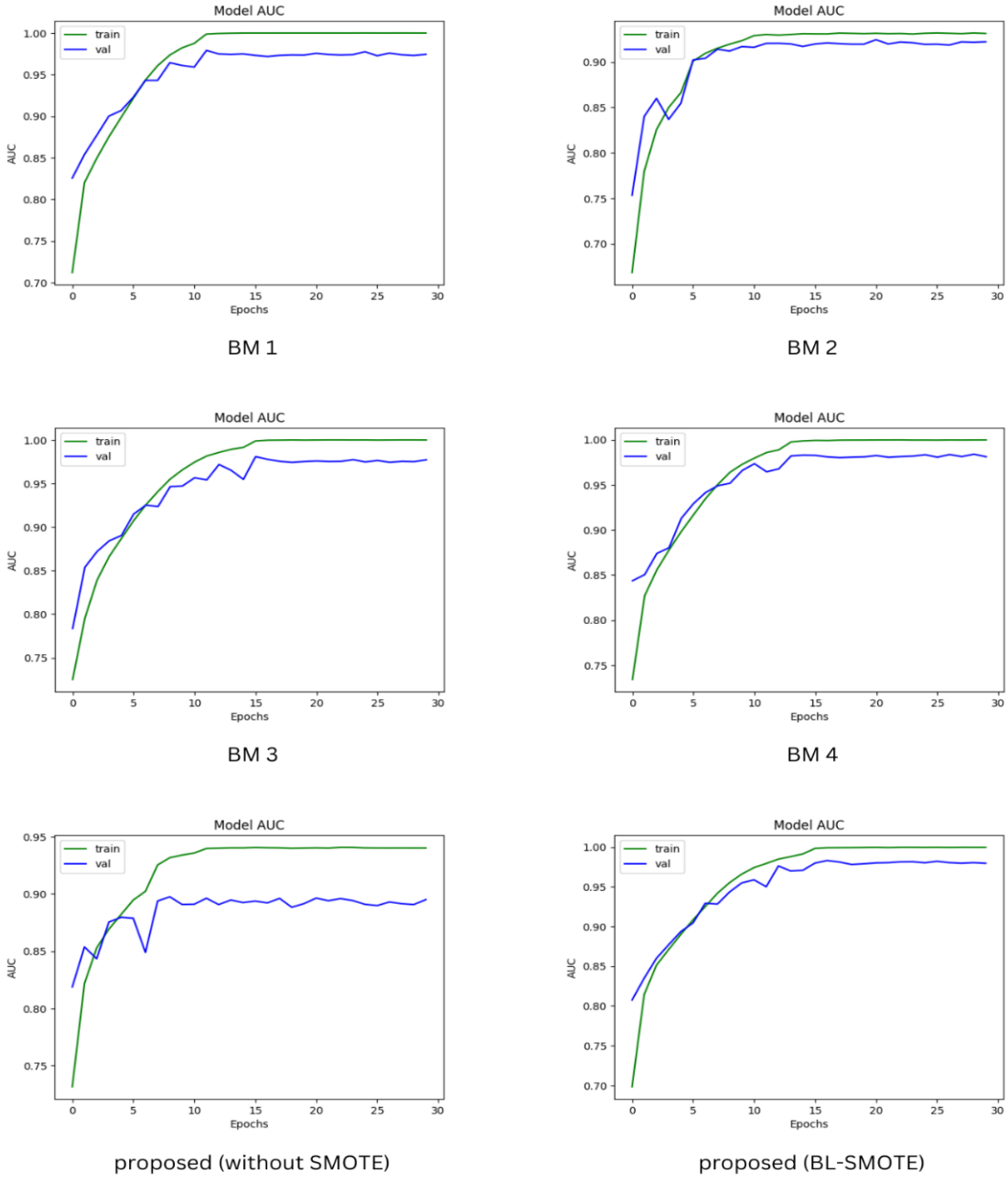

Figure 8. Analysis of Proposed X_R101 to baseline networks using the values of AUC (a) BM1 (b) BM2 (c) BM3 (d) BM4 (e) Proposed X_R101 before Borderline SMOTE, (f) Proposed X_R101 using Borderline SMOTE Tomek.

4.7. Precision of the Proposed X_R101 in Comparison to Other Classifiers

Using SMOTE TOMEK greatly improves the precision of the proposed X_R101. The proposed X_R101 models with and without BL-SMOTE achieved consistent precision values of 98.41%, and 93.10%. However, BM1, BM2, BM3, and BM4 had corresponding precision values of 92.26%, 93.93%, 95.60% and 96.72%. Figure 9 shows the main difference that was achieved in the proposed X_R101 by using the BL-SMOTE.

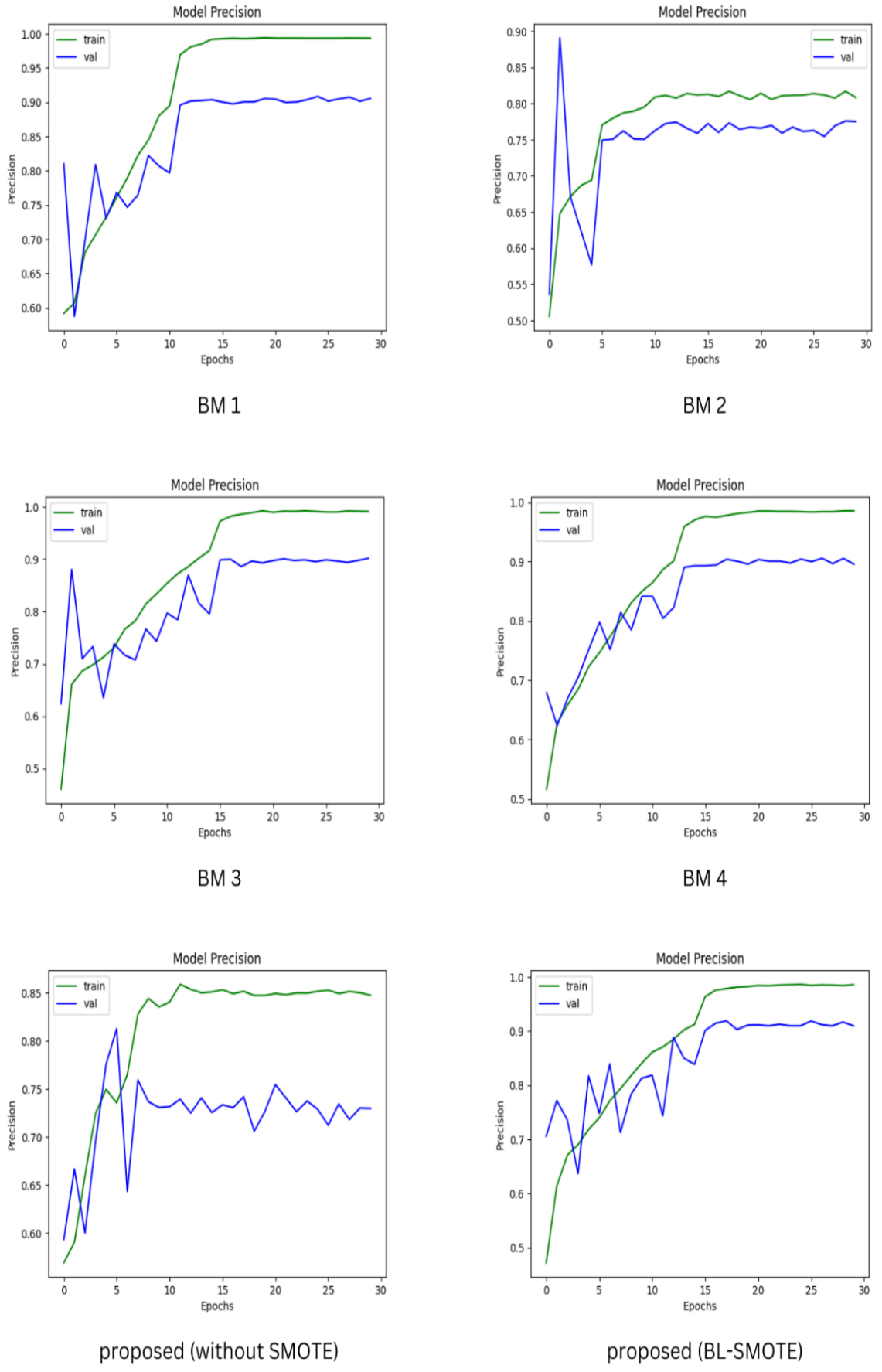

Figure 9. Assessment of Proposed X_R101 to baseline networks using precision (a) Xception, (b) ResNet-152, (c) MobileNet-V2, (d) Inception-V3, (e) Proposed X_R101 before BL SMOTE, (f) Proposed X_R101 using BL-SMOTE.

4.8. ROC of the Proposed X_R101 in Contrast to Baseline Networks

Utilizing BL-SMOTE substantially improves the precision of the proposed X_R101. In the presencence and absence of BL-SMOTE, the precision values for the X_R101 models were as follows: 98.45%, and 93.00 percent, respectively. On the other hand, the precision values corresponding to BM1, BM2, BM3, and BM4 were as follows: 92.56%, 94.12%, 95.50%, and 96.53%. The main differentiation introduced in the X_R101 prototype via the incorporation of the BL SMOTE is depicted in Figure 10.

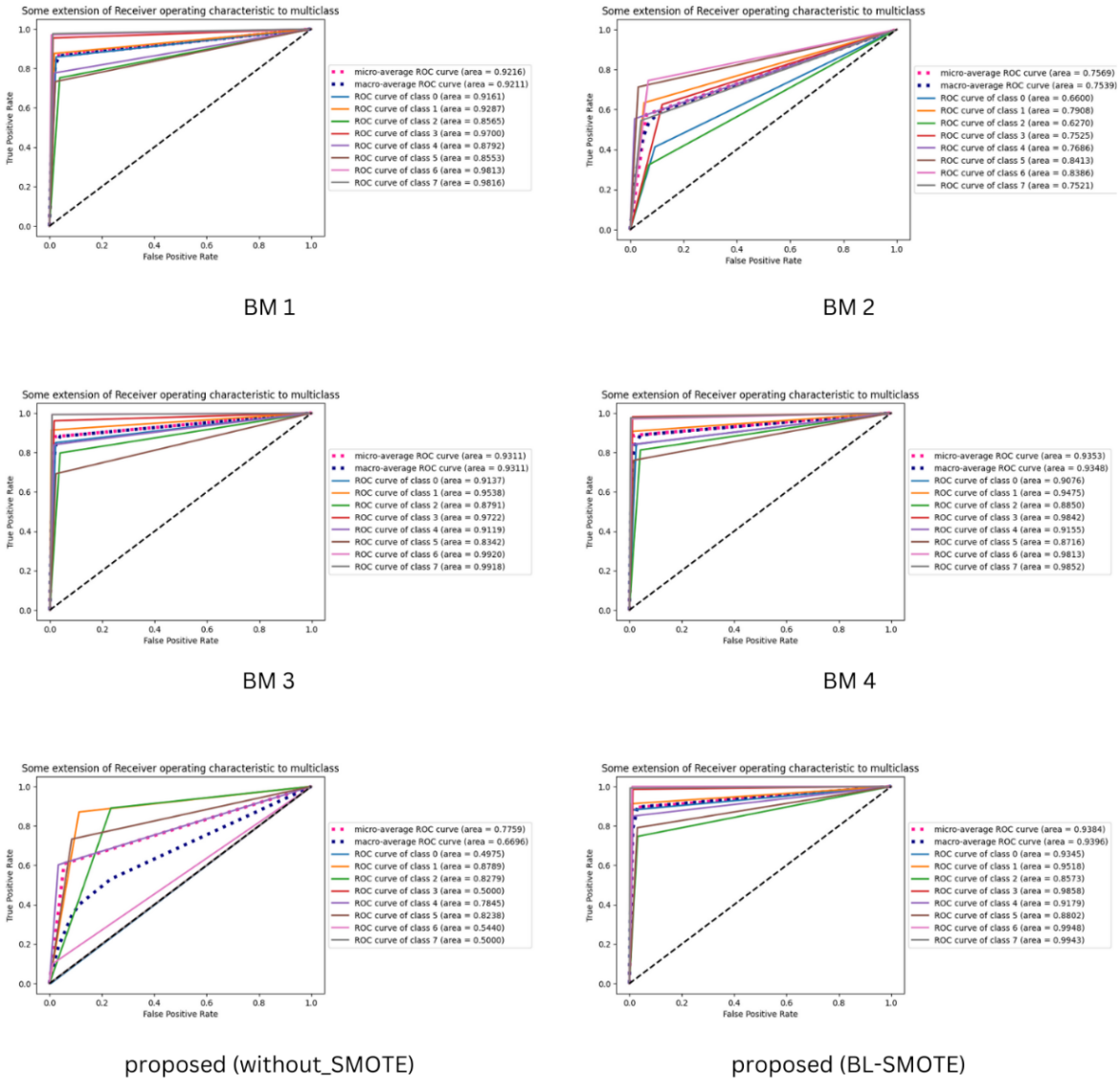

Figure 10. Evaluation of Proposed X_R101 to baseline networks using AUROC curve (a) Xception, (b) ResNet-152, (c) MobileNet-V2, (d) Inception-V3, (e) Proposed X_R101 before BL SMOTE, (f) Proposed X_R101 using BL-SMOTE..

4.9. Confusion Matrix of Proposed X_R101 to Other Classifiers

We validated our proposed X_R101 by comparing its results to those of four pre-existing networks using a confusion matrix. Significant enhancements were observed in the X_R101 model after the integration of BL SMOTE as depicted in Figure 11. Although X_R101 made an error in classifying eight case as Bk, three cases as Df, one as mel, three as Mn and one cases as Vasc, it successfully identified 118 instances of Ak. Similarly , the R_101 correctly indentify the 135 cases of Bcc whereas it misclassify 13 cases. In the case of Bk the X_R10 identify 103 instnaces correctly whereas 27 instances were wrongly classified. Furthermore, the X_R101 correctly classify 135 instances of Df and only two instances are misclassified. For Mel classification the proposed model correctly identify 130 cases and mis classify 23 cases. The X_R101 correctly identify the 102 cases of Mn and 27 cases are misclassified. For Scc and Vasc the proposed model

correctly classified 125 and 120 cases respectively. The results shows the outstanding performance of proposed method as compared to other baseline methods. An exhaustive summary of the results is presented in Figure 11.

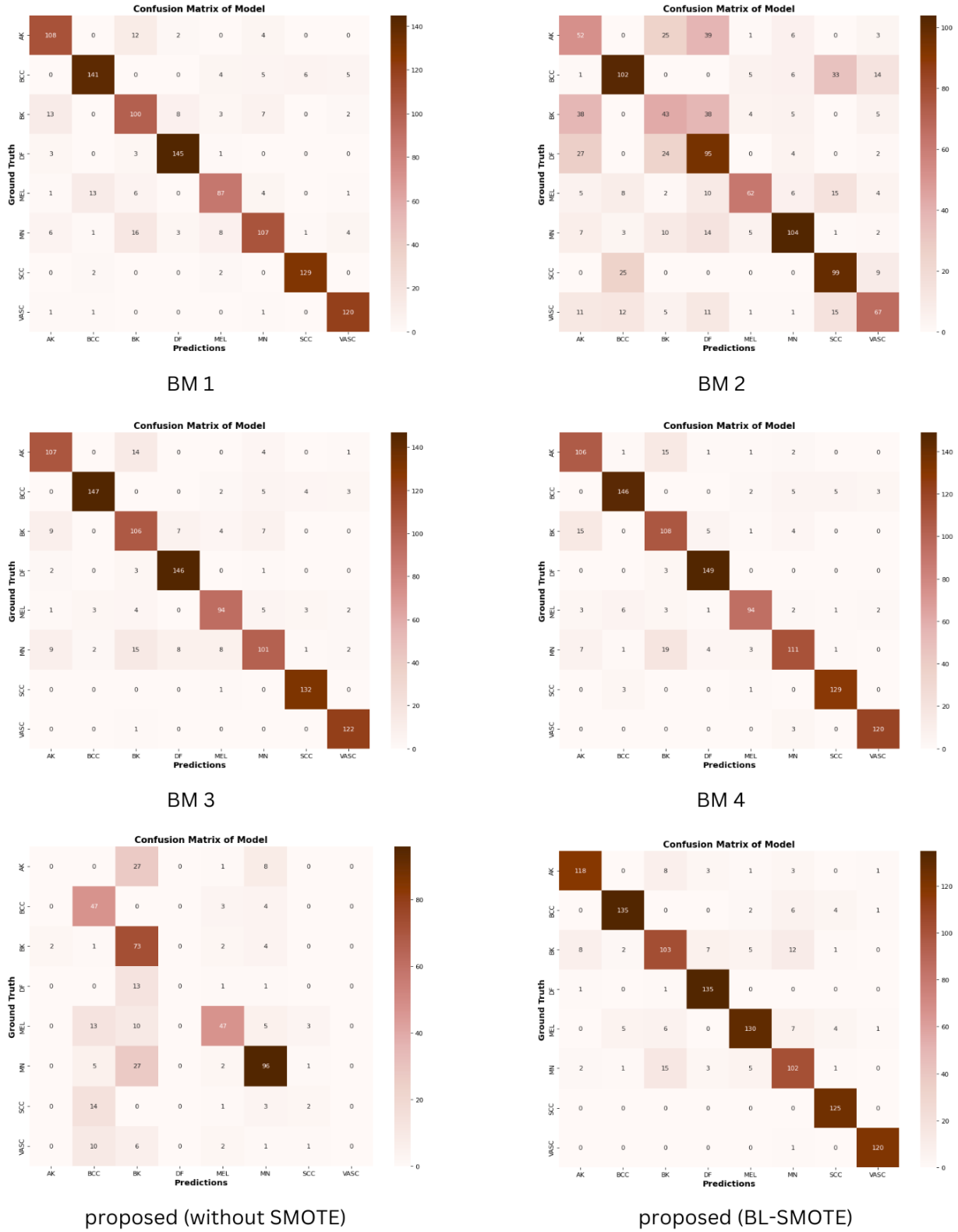

Figure 11. Confusion Matrix of Suggested X_R101 to baseline networks (a) BM1 (b) BM2 (c) BM3 (d) BM4 (e) Proposed X_R101 before Borderline SMOTE, (f) Proposed X_R101 using Borderline SMOTE Tomek.

4.10. Analysis of the Proposed X_R101 Utilizing State-of-the-Art

An examination of the proposed X_R101 model in relation to previous studies is discussed in this section [45-50]. Table 6 displays the results of a comprehensive assessment of the proposed X_R101 model across multiple performance metrics, including recall, accuracy, and F1-score.

Table 6. Comparison of the X-R101 in relation to the current SOTA

Ref	Year	Method	Dataset	Accuracy	Recall	Precision	F1
[45]	2023	Fuzzy+DL	ISIC 2018	95.90%	91.60%	97.40%	93.75%
[46]	2023	FCN-ResALexNet	ISIC 2018	94.65%	95.85%	87.86%	----
[47]	2023	ML+DL,	ISIC Archive	93.00%	93.76%	93.10%	----
[48]	2023	DSCC_Net	ISIC 2020, HAM10000 & DermPK	94.17%	95.00%	94.28%	93.93%
[49]	2022	ResNet+Naïve Bayes	HAM10000	85.50%	85.95%	85.73%	86.84%
[50]	2021	RCNN	ISIC 2017	95.20%	----	98.20%	----
Ours		Proposed X_R101 using BL SMOTE	PH2, DermPK & HAM10000	98.21%	98.41	98.33%	98.37%

4.12. Statistical Analysis of X_R101

In order to facilitate the comparison of X_R101, the statistical test of McNemar is utilised. The likelihood scores produced by the borderline classifiers were employed in the construction of the proposed model. In cases where the p-value corresponding to each sample instance is below 0.05, McNemar's test is restricted to confirming the null hypothesis by achieving a value of 0.0360. It is feasible to reject the null hypothesis on the basis of the findings derived from the statistical experiments. As a result, the X_R101 model exhibits a benefit over its rivals in terms of efficacy and includes utilization data that the others neglect to document. According to the results, the X_R101 model is significantly different from the others.

5. Discussions

The primary function of dermoscopy images is the detection of skin cancer. With the help of a finely detailed image of a particular area, a wide range of skin lesions can be identified. The utilization of a dermoscopy image capture method for the classification of Mel, Mn, Bcc, Scc, Vl, Ak, Df and Bk is a rapid, precise, and effective process. The implementation of an automated detection system was crucial for the timely identification of this critical condition, considering the increasing prevalence of skin cancer cases each day. At this time, dermoscopy images possess the capacity to diagnose a variety of diseases automatically due to the incorporation of artificial intelligence (AI). To facilitate the timely identification and management of skin cancer by medical practitioners, we have developed a CNN-based X_R101 model capable of precisely classifying dermoscopy images into the subsequent categories: Mel, Mn, Bcc, Scc, Vl, Ak, Df and Bk.

The experimental outcomes presented above provide evidence that the X_R101 model can effectively classify and train skin lesions of the following types: Mel, Mn, Bcc, Scc, Vl, Ak, Df and Bk. A comparison analysis of the four baseline classifiers proved that X_R101 performed greatly with a high accuracy rate of 98.21 % in its skin cancer detection application. We started the training procedure for BM1, BM2, BM3 and BM4 models with datasets of consistent resolution (224 x 224 x 3 pixels). In addition, the cross-entropy loss method was used during the training of the X-R101 model. The performance of the X_R101 model in Table 5 is demonstrated against the four baselines that were evaluated along the course of the study. The evaluation is carried out through a variety of metrics such as f1-score, recall, precision, and accuracy. The X_R101 model is really a good one as ROC of 0.9960, accuracy of 98.21%, precision of 98.41%, f1-score of 98.37%, and recall of 98.33% indicates.

The classification performance of the remaining four competitors' approaches, which utilized pre-trained weights, exhibited a marginal decline. With AUC scores of 0.9840, respectively, the BM4 classifier exhibited superior performance in performance evaluation when compared to the BM3, BM2, BM1 and

classifiers, which achieved a score of 0.98.16, 0.9829, 0.9834. BM4 demonstrates the highest AUC score (0. 9840), recall (96.79%), f1-score (96.73%), and precision (96.72%) among the models that were assessed. The overall binary classification problem was not impacted by the choice of pre-trained models based on CNN in a typical scenario. However, these systems exhibit limitations in their ability for multiclassifcation of diseases [12] and face cognitive challenges such as segmentation. As the number of CNN layers increases, the majority of researchers [30][37][40-45] consider convolutional neural network (CNN) classifiers inadequate for these particular binary classification tasks.

A comparison of the classification accuracy of contemporary classifiers and the X_R101 model is presented in Table 6. Based on empirical evidence and the application of modern techniques, it appears that the X_R101 model is capable of distinguisnig the following leisons: Mel, Mn, Bcc, Scc, Vl, Ak, Df and Bk. The clinical specialist has derived significant benefits from the dermoscopy images in relation to the infection.

Singh et al. [45] A modified deep learning model and a fuzzy logic-based image segmentation method are suggested for the purpose of diagnosing cutaneous cancer. The paper is noteworthy for its utilisation of mathematical logics, methodologies for calculating standard deviations, pre-processing to improve dermoscopy images, and the L-R fuzzy defuzzification technique to enhance the results of segmentation. To optimise the efficacy of deep convolutional neural network (CNN) architectures during the segmentation of skin lesions, a wide variety of metrics are utilised. Furthermore, for the segmentation of skin lesions, a novel deep learning architecture based on FCN (Fully Convolutional Network) is suggested by Ahmed et al. [46]. As previously mentioned, the decoder segment of the network consists of three deconvolutional layers. Conversely, the encoder architecture incorporates the highly regarded deep learning frameworks ResNet18 and AlexNet. Tembhurne et al. [47] presents an innovative approach to skin cancer detection that combines the fundamental tenets of deep learning and machine learning. Machine learning models examine image attributes that were obtained using techniques such as contourlet transform and local binary pattern histogram. On the other hand, deep learning models perform feature extraction from photographs by employing cutting-edge neural networks.

Tahir et al. [48] DSCC Net, a deep learning skin cancer detection system based on convolutional neural networks (CNNs), was assessed using three open-source benchmark datasets: ISIC 2020, HAM10000, and DermPK. Afza et al. [49] presents a structured architecture that utilizes deep learning and two-dimensional superpixels. the contrast of the initial dermoscopy images are enhanced through the integration of locally and globally augmented images. Following this, a comprehensive compilation of augmented images is utilized to segment skin lesions using a three-step superpixel lesion segmentation approach. Color images that are exclusively segmented are produced by utilizing each augmented dermoscopy image to map the lesions that have been segmented. These mapped images and acquired features are subsequently fed into a ResNet-50 deep learning model via transfer learning. The obtained features have been classified using the Naïve Bayes classifier, which has been trained using an enhanced grasshopper optimization approach. Nawaz et al. [50] proposed an approach that autonomously classifies early-stage skin cancers by integrating fuzzy k-means clustering (FKM) and quicker region-based convolutional neural networks (RCNN) within the domain of deep learning. The proposed methodology is evaluated using a wide range of clinical images in an effort to assist the dermatologist in promptly identifying this potentially life-threatening condition. Before implementing faster-RCNN to generate a fixed-length feature vector, the described method preprocesses the dataset images to rectify illumination and noise issues and enhance the visual information. Following that, epiDermPK afflicted by melanoma was sectioned into segments using FKM, which were distinguished by their clearly defined diameters and borders.

X_R101 exhibits superior capability in distinguishing among various classes of skin cancer through the extraction of dominant and discriminative patterns, as well as the detection of anomaly patterns, as evidenced by its highest accuracy result of 98.21% in Table 6. The outcomes of the final four baseline classifiers are also presented in Table 5. In addition to an examination of the features of Mel, Mn, Bcc, Scc, Vl, Ak, Df and Bk, we present a comprehensive clarification of the reasons behind the inferior classification performance of previous studies using dermoscopy images. The initial constraint on the classification performance of the CNN-based pre-trained classifiers is imposed by the deep networks and final convolutional (conv) layers, which minimize the spatial resolution of the feature map. Furthermore, the filter sizes of these pre-trained classifiers are inadequate due to the fact that their large input-connected

neurons immediately disregard crucial elements. The X_R101 model is capable of resolving these shortcomings. An end-to-end CNN-based model was developed with the assistance of Xception and resnet101. This model is capable of classifying diverse types of skin cancer from dermoscopy images collected from multiple databases. The accuracy issue of low resolution and overlapping in dermoscopy images' inflammatory segment has been solved by using the X_R101 model. Also, the model is able to speed up the classification performance and is effective in minimizing the adverse effects of structured noise. Therefore, the X_R101 model was equipped with the appropriate filter size of 3x3. The findings of the experiment illustrate that the X_R101 method can accurately do the multiclassification of Mel, Mn, Bcc, Scc, Vl, Ak, Df & Bk and helps the healthcare practitioners.

6. Conclusion

The goal of our research is to identify a methodology that can simultaneously enhance the accuracy of skin cancer detection and reduce the occurrence of false positive outcomes. Therefore, in order to improve the timely detection of skin cancer, we present a novel deep-learning architecture that integrates the functionalities of Xception and ResNet101. The X_R101 exhibits remarkable performance with regard to the classification of Mel, Mn, Bcc, Scc, Vl, Ak, Df and Bk. To evaluate the efficacy of the X_R101 model, its classification accuracy was compared to that of four reference models. The identified skin cancer was successfully detected by the proposed model, which achieved a success rate of 98.21%. The findings of this study indicate that the X_R101 model with BL SMOTE for the multiclassification of skin cancer utilizing dermoscopy images in an efficient method. The McNemar statistical test validates the efficetive performance of the proposed X_R101. The results benefits the medical practitioners who rely on particular diagnostic attributes derived from imaging and enhance their capacity when employing dermoscopy for the detection of diverse forms of skin cancer. Moreover, we anticipate that more comprehensive datasets containing patients who have been diagnosed with skin cancer will be made available to the public. The inclusion of more publically available datasets will significantly improve the accuracy of our proposed network. The proposed procedure is expected to enhance dermatologist ability to rapidly detect and differentiate between various types of skin malignancies. This study advances the early identification and diagnosis of skin cancer, which has important treatment implications for further laboratory investigations. Additionally, a significant reduction in the costs related to the detection of the critical condition may help alleviate the financial burden.

Funding: This research received no external funding.

Conflict of Interest: The author declares no conflict of interest

References

1. Ahmed, A. M., Ahmed, M. H., Saha, S. K., Ahmed, O., & Sutradhar, A. (2022). Optimization algorithms as training approach with hybrid deep learning methods to develop an ultraviolet index forecasting model. Stochastic Environmental Research and Risk Assessment, 36(10), 3011-3039.
2. Lee, C., Yoo, S., Lee, H. N., & Lee, J. (2023). DeepErythema: A Study on the Consistent Evaluation Method of UV SPF Index through Deep Learning. IEEE Access.
3. Mazhar, T., Haq, I., Ditta, A., Mohsan, S. A. H., Rehman, F., Zafar, I., ... & Goh, L. P. W. (2023, February). The role of machine learning and deep learning approaches for the detection of skin cancer. In Healthcare (Vol. 11, No. 3, p. 415). MDPI.
4. Zia Ur Rehman, M., Ahmed, F., Alsuhibany, S. A., Jamal, S. S., Zulfiqar Ali, M., & Ahmad, J. (2022). Classification of skin cancer lesions using explainable deep learning. Sensors, 22(18), 6915.
5. Agrahari, P., Agrawal, A., & Subhashini, N. (2022). Skin cancer detection using deep learning. In Futuristic Communication and Network Technologies: Select Proceedings of VICFCNT 2020 (pp. 179-190). Springer Singapore.
6. Alwakid, G., Gouda, W., Humayun, M., & Sama, N. U. (2022, December). Melanoma detection using deep learning-based classifications. In Healthcare (Vol. 10, No. 12, p. 2481). MDPI.
7. Riaz, S., Naeem, A., Malik, H., Naqvi, R. A., & Loh, W. K. (2023). Federated and Transfer Learning Methods for the Classification of Melanoma and Nonmelanoma Skin Cancers: A Prospective Study. Sensors, 23(20), 8457.
8. Gouda, W., Sama, N. U., Al-Waakid, G., Humayun, M., & Jhanjhi, N. Z. (2022, June). Detection of skin cancer based on skin lesion images using deep learning. In Healthcare (Vol. 10, No. 7, p. 1183). MDPI
9. Mirikharaji Z, Abhishek K, Bissoto A, Barata C, Avila S, Valle E, Celebi ME, Hamarneh G. A survey on deep learning for skin lesion segmentation. Medical Image Analysis. 2023 Jun 9:102863.
10. Kousis, I., Perikos, I., Hatzilygeroudis, I., & Virvou, M. (2022). Deep learning methods for accurate skin cancer recognition and mobile application. Electronics, 11(9), 1294.
11. Sharma, A. K., Tiwari, S., Aggarwal, G., Goenka, N., Kumar, A., Chakrabarti, P., ... & Jasiński, M. (2022). Dermatologist-level classification of skin cancer using cascaded ensembling of convolutional neural network and handcrafted features based deep neural network. IEEE Access, 10, 17920-17932.
12. Naeem, A., Farooq, M. S., Khelifi, A., & Abid, A. (2020). Malignant melanoma classification using deep learning: datasets, performance measurements, challenges and opportunities. IEEE access, 8, 110575-110597.
13. Khalil, M., Naeem, A., Naqvi, R. A., Zahra, K., Muqarib, S. A., & Lee, S. W. (2023). Deep learning-based classification of abrasion and ischemic diabetic foot sores using camera-captured images. Mathematics, 11(17), 3793.
14. Naeem, A., Anees, T., Naqvi, R. A., & Loh, W. K. (2022). A comprehensive analysis of recent deep and federated-learning-based methodologies for brain tumor diagnosis. Journal of Personalized Medicine, 12(2), 275.
15. Malik, H., Anees, T., Din, M., & Naeem, A. (2023). CDC_Net: Multi-classification convolutional neural network model for detection of COVID-19, pneumothorax, pneumonia, lung Cancer, and tuberculosis using chest X-rays. Multimedia Tools and Applications, 82(9), 13855-13880.
16. Malibari, A. A., Alzahrani, J. S., Eltahir, M. M., Malik, V., Obayya, M., Al Duhayyim, M., ... & de Albuquerque, V. H. C. (2022). Optimal deep neural network-driven computer aided diagnosis model for skin cancer. Computers and Electrical Engineering, 103, 108318.
17. Akilandasowmya, G., Nirmaladevi, G., Suganthi, S. U., & Aishwariya, A. (2024). Skin cancer diagnosis: Leveraging deep hidden features and ensemble classifiers for early detection and classification. Biomedical Signal Processing and Control, 88, 105306.
18. Nirmala, V. (2023). An automated detection of notable ABCD diagnostics of melanoma in dermoscopic images. In Artificial Intelligence in Telemedicine (pp. 67-82). CRC Press.
19. Zafar, M., Sharif, M. I., Sharif, M. I., Kadry, S., Bukhari, S. A. C., & Rauf, H. T. (2023). Skin lesion analysis and cancer detection based on machine/deep learning techniques: A comprehensive survey. Life, 13(1), 146.
20. Das, J. B. A., Mishra, D., Das, A., Mohanty, M. N., & Sarangi, A. (2022, November). Skin cancer detection using machine learning techniques with ABCD features. In 2022 2nd Odisha International Conference on Electrical Power Engineering, Communication and Computing Technology (ODICON) (pp. 1-6). IEEE.
21. Shah, A., Shah, M., Pandya, A., Sushra, R., Sushra, R., Mehta, M., ... & Patel, K. (2023). A comprehensive study on skin cancer detection using artificial neural network (ANN) and convolutional neural network (CNN). Clinical eHealth.
22. Reshma, G., Al-Atroshi, C., Nassa, V. K., Geetha, B. T., Sunitha, G., Galety, M. G., & Neelakandan, S. (2022). Deep learning-based skin lesion diagnosis model using dermoscopic images. Intelligent Automation & Soft Computing, 31(1).
23. Mampitiya, L. I., Rathnayake, N., & De Silva, S. (2023). Efficient and low-cost skin cancer detection system implementation with a comparative study between traditional and CNN-based models. Journal of Computational and Cognitive Engineering, 2(3), 226-235.
24. Jones, O. T., Matin, R. N., van der Schaar, M., Bhayankaram, K. P., Ranmuthu, C. K. I., Islam, M. S., ... & Walter, F. M. (2022). Artificial intelligence and machine learning algorithms for early detection of skin cancer in community and primary care settings: a systematic review. The Lancet Digital Health, 4(6), e466-e476.
25. Ph2 dataset available online: https://www.fc.up.pt/addi/ph2%20database.html , Accessed on 23 feb 2024
26. Dermpk dataset available online https://data.mendeley.com/datasets/fdhyjjypbd/1 , Accessed on 23 feb 2024

27. Ham10000 dataset available online https://www.kaggle.com/datasets/surajghuwalewala/ham1000-segmentation-and-classification , Accessed on 23 feb 2024
28. Kassem, M. A., Hosny, K. M., & Fouad, M. M. (2020). Skin lesions classification into eight classes for ISIC 2019 using deep convolutional neural network and transfer learning. IEEE Access, 8, 114822-114832.
29. Abbas, Q., Ramzan, F., & Ghani, M. U. (2021). Acral melanoma detection using dermoscopic images and convolutional neural networks. Visual Computing for Industry, Biomedicine, and Art, 4, 1-12.
30. Reis, H. C., Turk, V., Khoshelham, K., & Kaya, S. (2022). InSiNet: a deep convolutional approach to skin cancer detection and segmentation. Medical & Biological Engineering & Computing, 1-20.
31. Monika, M. K., Vignesh, N. A., Kumari, C. U., Kumar, M. N. V. S. S., & Lydia, E. L. (2020). Skin cancer detection and classification using machine learning. Materials Today: Proceedings, 33, 4266-4270.
32. Ibraheem, M. R., & Elmogy, M. (2020, October). A non-invasive automatic skin cancer detection system for characterizing malignant melanoma from seborrheic keratosis. In 2020 2nd International Conference on Computer and Information Sciences (ICCIS) (pp. 1-5). IEEE.
33. Rehman, M., Khan, S. H., Rizvi, S. D., Abbas, Z., & Zafar, A. (2018, July). Classification of skin lesion by interference of segmentation and convolotion neural network. In 2018 2nd International Conference on Engineering Innovation (ICEI) (pp. 81-85). IEEE.
34. Shetty, B., Fernandes, R., Rodrigues, A. P., Chengoden, R., Bhattacharya, S., & Lakshmanna, K. (2022). Skin lesion classification of dermoscopic images using machine learning and convolutional neural network. Scientific Reports, 12(1), 18134.
35. Agyenta, C., & Akanzawon, M. (2022). Skin Lesion Classification Based on Convolutional Neural Network. Journal of Applied Science and Technology Trends, 3(01), 14-19.
36. Naeem, A., Anees, T., Fiza, M., Naqvi, R. A., & Lee, S. W. (2022). SCDNet: A Deep Learning-Based Framework for the Multiclassification of Skin Cancer Using Dermoscopy Images. Sensors, 22(15), 5652.
37. Zambrano-Román, M., Padilla-Gutiérrez, J. R., Valle, Y., Muñoz-Valle, J. F., & Valdés-Alvarado, E. (2022). Non-Melanoma Skin Cancer: A Genetic Update and Future Perspectives. Cancers, 14(10), 2371.
38. Han, H., Wang, W. Y., & Mao, B. H. (2005, August). Borderline-SMOTE: a new over-sampling method in imbalanced data sets learning. In International conference on intelligent computing (pp. 878-887). Berlin, Heidelberg: Springer Berlin Heidelberg.
39. Goceri, E. (2023). Evaluation of denoising techniques to remove speckle and Gaussian noise from dermoscopy images. Computers in Biology and Medicine, 152, 106474.
40. Mehmood, A., Gulzar, Y., Ilyas, Q. M., Jabbari, A., Ahmad, M., & Iqbal, S. (2023). SBXception: a shallower and broader xception architecture for efficient classification of skin lesions. Cancers, 15(14), 3604.
41. Mohapatra, S., Abhishek, N. V. S., Bardhan, D., Ghosh, A. A., & Mohanty, S. (2021). Comparison of MobileNet and ResNet CNN Architectures in the CNN-Based Skin Cancer Classifier Model. Machine Learning for Healthcare Applications, 169-186.
42. Mehra, A., Bhati, A., Kumar, A., & Malhotra, R. (2021). Skin cancer classification through transfer learning using ResNet-50. In Emerging Technologies in Data Mining and Information Security: Proceedings of IEMIS 2020, Volume 2 (pp. 55-62). Singapore: Springer Nature Singapore.
43. Budhiman, A., Suyanto, S., & Arifianto, A. (2019, December). Melanoma cancer classification using resnet with data augmentation. In 2019 International Seminar on Research of Information Technology and Intelligent Systems (ISRITI) (pp. 17-20). IEEE.
44. Demir, A., Yilmaz, F., & Kose, O. (2019, October). Early detection of skin cancer using deep learning architectures: resnet-101 and inception-v3. In 2019 medical technologies congress (TIPTEKNO) (pp. 1-4). IEEE.
45. Singh, S. K., Abolghasemi, V., & Anisi, M. H. (2023). Fuzzy logic with deep learning for detection of skin cancer. Applied Sciences, 13(15), 8927.
46. Ahmed, N., Tan, X., & Ma, L. (2023). A new method proposed to Melanoma-skin cancer lesion detection and segmentation based on hybrid convolutional neural network. Multimedia Tools and Applications, 82(8), 11873-11896.
47. Tembhurne, J. V., Hebbar, N., Patil, H. Y., & Diwan, T. (2023). Skin cancer detection using ensemble of machine learning and deep learning techniques. Multimedia Tools and Applications, 1-24.
48. Tahir, M., Naeem, A., Malik, H., Tanveer, J., Naqvi, R. A., & Lee, S. W. (2023). DSCC_Net: Multi-Classification Deep Learning Models for Diagnosing of Skin Cancer Using Dermoscopic Images. Cancers, 15(7), 2179.
49. Afza, F., Sharif, M., Mittal, M., Khan, M. A., & Hemanth, D. J. (2022). A hierarchical three-step superpixels and deep learning framework for skin lesion classification. Methods, 202, 88-102.
50. Nawaz, M., Mehmood, Z., Nazir, T., Naqvi, R. A., Rehman, A., Iqbal, M., & Saba, T. (2022). Skin cancer detection from dermoscopic images using deep learning and fuzzy k-means clustering. Microscopy research and technique, 85(1), 339-351.